Atmospheric Reflection during an Anomalous Low State of Hercules X-1

Still, M.; O' Brien, K.; Horne, K.; Boroson, B.; Titarchuk, L.G.; Engle, K.; Vrtilek, S.D.; Quaintrell, H.; Fiedler, H.

Published in:
Astrophysical Journal

DOI:
10.1086/321337

THE ASTROPHYSICAL JOURNAL, 554:352–361, 2001 June 10

ATMOSPHERIC REFLECTION DURING AN ANOMALOUS LOW STATE OF HERCULES X-1

MARTIN STILL[1]
NASA Goddard Space Flight Center, Code 662, Greenbelt, MD 20771; School of Physics and Astronomy, University of St. Andrews, North Haugh, St. Andrews, Fife KY16 9SS, UK

KIERAN O'BRIEN, AND KEITH HORNE
School of Physics and Astronomy, University of St. Andrews, North Haugh, St. Andrews, Fife KY16 9SS, UK

BRAM BOROSON, LEV G. TITARCHUK, AND KIMBERLY ENGLE[2]
NASA Goddard Space Flight Center, Greenbelt, MD 20771

SAEQA D. VRTILEK
Harvard-Smithsonian Center for Astrophysics, 60 Garden Street, Cambridge, MA 02138

HANNAH QUAINTRELL
Department of Physics, The Open University, Milton Keynes MK7 6AA, UK

AND

HAUKE FIEDLER
Institute of Astronomy and Astrophysics, Ludwig-Maximilian University, D-81679 Munich, Germany
Received 2000 October 10; accepted 2001 January 23

ABSTRACT

We present *RXTE* observations of the eclipsing X-ray binary Hercules X-1 during an anomalous low state. Data reduction reveals a light curve over 2.7 orbital cycles remarkably similar to optical and UV light curves dominated by the companion star. Count rates are modulated close to the orbital period, attaining a maximum when the inner face of the companion star, irradiated by X-rays from the compact source, is most visible. Cold reflection provides an acceptable fit to the energy spectrum. Employing binary geometry to scale the model and assuming companion-star reflection, we are able to reconstruct the incident X-rays that are removed from our direct line of sight (presumably by the accretion disk). We find the flux of the hidden source to be identical to the observed flux of Her X-1 at the peak of its main high state. Consequently, Her X-1 is emitting a reflected spectrum, largely uncontaminated by direct X-rays in the anomalous low state. The spectral energy distribution, period, amplitude, and phasing of the modulation are all consistent with a companion-star origin. Since this source occurs in a well-understood binary environment, it provides an excellent case study for more sensitive experiments in the future.

Subject headings: binaries: close — binaries: eclipsing — pulsars: individual (Hercules X-1) — radiative transfer — stars: neutron — X-rays: stars

1. INTRODUCTION

Her X-1 (Tananbaum et al. 1972) is an eclipsing X-ray binary containing a pulsar of 1.4 $M_\odot$ and an A7 stellar companion of 2.2 $M_\odot$ (Middleditch & Nelson 1976; Reynolds et al. 1997). The system displays behavior on four separate periods: the pulsar spin (1.24 s), the binary orbit (1.7 days), a superperiod of 35 days, which results from a retrograde, precessing, warped accretion disk, and a beat between the precessional and orbital periods of 1.62 days. The warp phenomenon is poorly understood, but its source is likely to be a combination of both tide- and radiation-driven precession (Papaloizou & Terquem 1995; Pringle 1996).

The 35 day supercycle results in two phases of strong X-ray activity per cycle (Giacconi et al. 1973; Scott & Leahy 1999). The main high state has a rapid turn-on over $\sim$90 m and decays over $\sim$10 days. An off state where flux remains at $\sim$1% of the high-state level follows for the next $\sim$10 days, succeeded by a second short high state lasting $\sim$5 days, with flux peaking at $\sim$30% of maximum. A further off state completes the cycle and extends over the next $\sim$10 days. The accretion disk casts a shadow that migrates across the surface of the companion star on the beat frequency. The supercycle is consequently observed at UV and optical energies, which are dominated by X-ray emission reprocessed in the stellar atmosphere (Gerend & Boynton 1976).

The 35 day clock has remained mostly coherent since its discovery. There have been three occasions, however, when the clock has missed several consecutive turn-ons or its main high-state flux has been reduced (Parmar et al. 1985; Vrtilek et al. 1994; Oosterbroek et al. 2000). The cause of these anomalous low states is not clear, but they probably result from changes in the state of the accretion disk, through either an increase in vertical scale height or disruption of the disk warp. Whatever the cause, the level of reprocessed UV and optical flux from the companion star during these states suggests that the intrinsic X-ray flux and (presumably) the accretion rate remain mostly unaffected (Vrtilek et al. 1994, 2001). The high orbital inclination of the binary indicates that perhaps just a small variation in the disk geometry will block direct X-rays from our line of sight, while the companion star's view remains largely unchanged over much of its surface area.

The latest anomalous low state began during 1999 February (Oosterbroek et al. 2000), and the on states had not recovered four cycles later, when the current observations

[1] Universities Space Research Association.
[2] Science Systems and Applications, Inc. (SSAI), 5900 Princess Garden Parkway, Suite 300, Lanham, MD 20706.

were scheduled. These were part of a simultaneous multiwavelength campaign on Her X-1 described by Vrtilek et al. (2001). Results from simultaneous *Hubble Space Telescope* orbits are detailed by Boroson et al. (2000a, 2000b), and an earlier epoch of short high-state visits with *RXTE* is presented by Still et al. (2001).

The current *RXTE* data reveal many similarities between the X-ray light curve and its optical/UV counterparts, suggesting that much of the anomalous low-state X-ray emission could be of companion-star origin. We find that cold Compton reflection is a statistically acceptable model for the energy spectrum, and a reflection surface the size and distance from the pulsar of the companion star gives a good prediction of the incident X-ray flux, provided this is identical to the peak of the normal on-state intensity. The possible detection of a relatively clean reflection spectrum in a well-determined binary geometry, free of dominant direct X-rays, would be a valuable resource for investigators of reflecting atmospheres in the less well-determined environments of active galactic nuclei (AGNs) and stellar black hole candidates (Lightman & White 1988; White, Lightman, & Zdziarski 1988).

2. OBSERVATIONS

RXTE pointed at Her X-1 intermittently between 1999 July 11 and 16 (MJD 51,370.83–51,375.37), accumulating 100 ks of time-tagged events. Event reconstruction was performed using standard algorithms within FTOOLS v. 4.2. We analyzed data from the Proportional Counter Array (PCA; Zhang et al. 1993), in which three of the five identical Xe Proportional Counting Units (PCUs) were operational with a combined effective area of 3900 cm^2. As well as the standard data formats, we employed two event analyzers in the GoodXenon event mode with 2 s readout—time stamps were resolved to 1 μs, while employing the full 256 energy channels (2.2–119.0 keV during epoch 4). Response matrices from 1999 March 30 were obtained from the HEASARC archive.[3] Background estimates are derived from the Very Large Event model[4] to account for cosmic events, internal particle generation, and South Atlantic Anomaly activation. Events from the High-Energy X-ray Timing Experiment (HEXTE), also on board the spacecraft, proved too scarce to be useful.

Throughout this paper we will employ the orbital ephemeris of Deeter et al. (1991),

$$T_{\rm orb} = \text{MJD } 43{,}804.51998(1) + 1.70016772(1)E_{\rm orb} - 5.2(5) \times 10^{-11}E_{\rm orb}^2 , \quad (1)$$

where $T_{\rm orb}$ corresponds to superior conjunction of the compact star and $E_{\rm orb}$ is the orbital cycle number. Assuming that the 35 day epoch is determined by

$$T_{35} = \text{MJD } 50{,}041.0 + 34.85E_{35} , \quad (2)$$

where T_{35} corresponds to X-ray turn-on of the main high state and E_{35} is the cycle number (M. Kunz 2000, private communication), the precession phases sampled are $\phi_{35} =$ 0.16–0.29. These would normally correspond approximately to the second half of a main high state (Scott & Leahy 1999), but the average count rate of 4 counts s^{-1} PCU^{-1} testifies to the anomalous extended low state in which Her X-1 had remained for the previous four 35 day cycles (Coburn et al. 2000). Count rates are of order 1% of the normal high state (Dal Fiume et al. 1998).

[3] Available at http://xte.gsfc.nasa.gov.

[4] Available at http://www.denison.edu/~stark/pca/pcabackest.html.

3. LIGHT CURVE

Standard2 data from each visit were filtered to reject pointings closer than 10° to the Earth's limb and those off axis by 0.°02 or more. From all PCA layers and columns, events were summed across pulse-height channels to provide a light curve in the energy range 3–30 keV with 1 ks sampling. This is presented in Figure 1, and hardness ratios for 2–5 keV, 5–8 keV, and 8–20 keV bands are provided in Figure 2 (eclipse data have been removed from the hardness diagrams). Background models have been subtracted and data divided by the number of active PCUs.

Gerend & Boynton (1976) show that the majority of power from companion-star emission occurs on the 1.7 day orbital frequency, through stellar rotation. However, light-

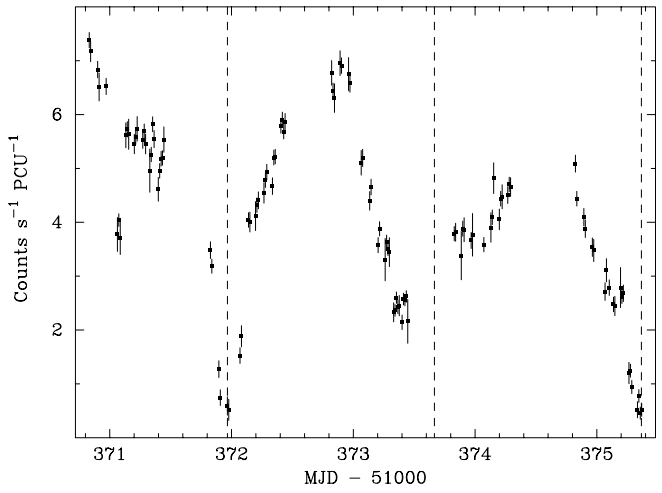

FIG. 1.—The 3–30 keV band light curve over the duration of the observations. Vertical dashed lines correspond to superior conjunction of the neutron star, according to the orbital ephemeris of Deeter et al. (1991).

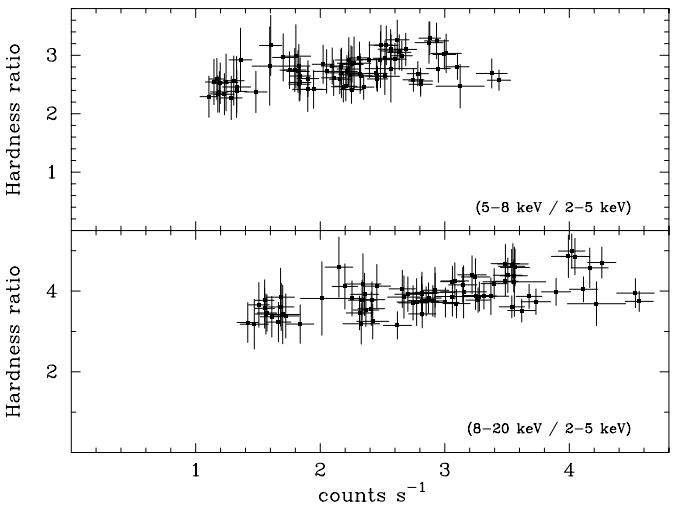

FIG. 2.—Hardness ratios for the 2–5 keV, 5–8 keV, and 8–20 keV bands. Eclipse points, $\phi_{\rm orb} = -0.1$–0.1, have been excluded.

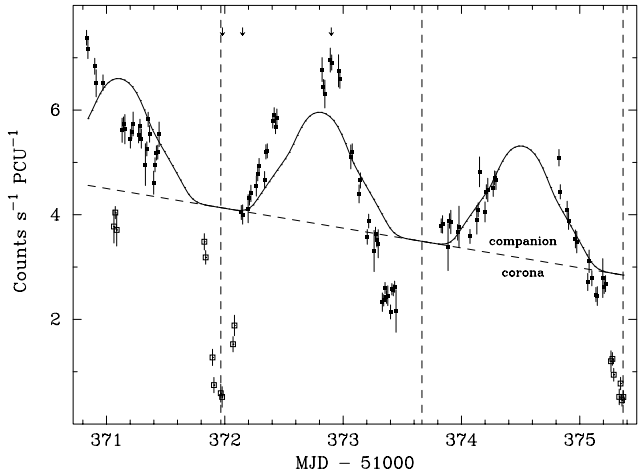

FIG. 3.—Fit to the light curve using the geometric binary synthesis code of Still et al. (1997) plus a linear decay function to represent the corona. Points designated by open squares, corresponding to eclipses and the dip at MJD 51,371.05, were ignored by the fit. The dashed line is the coronal fit alone. The three spectra presented in Fig. 4 were extracted from the visits indicated by arrows.

curve structures associated with the accretion flow from the companion star, such as the hot spot and splash from the collision of stream and disk (Schandl 1996), occur on a timescale close to the beat period. Figure 1 shows an intensity modulation approximating the 1.7 day orbital period. Depending on its source, we expect the observed modulation to occur in either the orbital or the 1.62 day beat period.

The hardness ratios of Figure 2 indicate that the modulation is not the result of photoelectric absorption. We are observing intrinsic flux increases or opaque obstruction of a soft emission region. The observed structure occurs over timescales several factors longer than normal main high-state dipping events (Leahy 1997).

Maximum flux corresponds approximately with orbital phase $\phi_{\rm orb} = 0.5$, where $\phi_{\rm orb} = 0.0$ is superior conjunction of the neutron star. This is consistent with a region associated with the irradiated inner surface of the companion star. The similarities between this light curve and the optical, UV, and EUV light curves, which are dominated by companion-star emission, are striking (Still et al. 1997; Leahy & Marshall 1999; Boroson et al. 2000a). We suggest that the modulation is the result of Compton reflection of X-rays off the atmosphere of the companion, as predicted by Basko, Sunyaev, & Titarchuk (1974) and detected at EUV wavelengths by Leahy & Marshall (1999) and Leahy, Marshall, & Scott (2000).

If we are detecting companion-star reflection, there must be a second source of X-ray flux associated with the compact object in order to produce the narrow eclipses at MJD 51,372.0, MJD 51,373.7, and MJD 51,375.4. There are equivalent eclipses at optical and UV wavelengths that are thought to be the eclipse of disk light by the companion star (Gerend & Boynton 1976; Boroson et al. 2000a).

After removing eclipses and using the Lomb-Scargle statistic (Scargle 1982), the best-fit period to this light curve is 1.74 ± 0.06 days, with a false-alarm probability of 10^{-12}. The error is the σ-width of the peak in the power spectrum and can only discriminate between the orbital and beat frequencies to 1.3 σ.

We attempt a crude fit to the light curve in which the reflection component is constructed by combining the geometric stellar synthesis code of Still et al. (1997) with the classical H function reflection coefficients (Chandrasekhar 1960). Reflected flux between 3 and 30 keV is integrated over the stellar surface area. This is detailed in the Appendix. We adopt an orbital inclination of $i = 82°$, a neutron star mass of $M_{\rm ns} = 1.4\ M_\odot$, and a Roche lobe-filling companion-star mass of $M_{\rm com} = 2.2\ M_\odot$ (Reynolds et al. 1997). Unlike Still et al. (1997), and in order to reduce the number of free parameters, we do not attempt to model the shadow of the accretion disk over the companion star or the orbital eclipse of the star by the disk, centered at $\phi_{\rm orb} = 0.5$. The energy spectrum of the compact source is taken to be a power law of slope $\alpha = 0.9$ with an exponential cutoff at $E_{\rm cut} = 11$ keV (see § 4). The luminosity of the source is arbitrary, where the resulting reflection spectrum is rescaled such that the maximum count rate at $\phi_{\rm orb} = 0.5$ is 1 count s^{-1} PCU^{-1}. The coronal component is represented by a linear function—a better fit statistically than using a constant—such that the overall fit is given by

$$L(t) = p_1 + p_2\, t + p_3\, R(t)\,, \tag{3}$$

where p_1 and p_2 are the constant and linear terms of the coronal component, p_3 is a renormalization constant for the modeled companion-star light curve $R(t)$, and t is time in days after MJD 51,000.

After the eclipse points and the dip at MJD 51,371.05 were rejected, the fit was made using a Downhill Simplex Algorithm (Press et al. 1992). The result is plotted in Figure 3, where $p_1 = 145$, $p_2 = -0.38$, and $p_3 = 2.14$; $\chi^2 = 2100$ for 84 degrees of freedom (dof). Decreasing coronal flux is consistent with the behavior of direct photons from the accretion region during this phase of the normal 35 day cycle (Scott & Leahy 1999).

The fit is poor, although this is not particularly discouraging given our first-order treatment of coronal variability. Residuals are probably dominated by the coronal component. In the following sections we perform spectral fits in an attempt to separate the two components, test the suitability of reflection for fitting the energy spectrum of the modulated component, and subtract modeled stellar reflection spectra to reveal the spectral variability of the corona.

4. ENERGY SPECTRUM

Under the same filtering constraints as above, the GoodXenon events were sampled with the full pulse-height resolution of the PCA. Channels 1–7 (<3 keV) were ignored because of uncertain background modeling, and channels 63–256 (>30 keV) were ignored as a result of poor counting statistics. XSPEC v. 11 was used at all times. Spectral fits to three of the visits are presented in Figure 4.

4.1. *Corona Spectrum*

We consider a model in which emission originates from two distinct binary regions, an accretion disk corona and the companion star. We first consider the corona, whose output is presumably the result of upscattering soft disk photons in a relatively hot medium (see, e.g., Sunyaev & Titarchuk 1980). For now, the parameters of this model will be considered constant over time (excluding eclipses), except for the normalization parameter, which we will vary according to the linear component of our light-curve fit

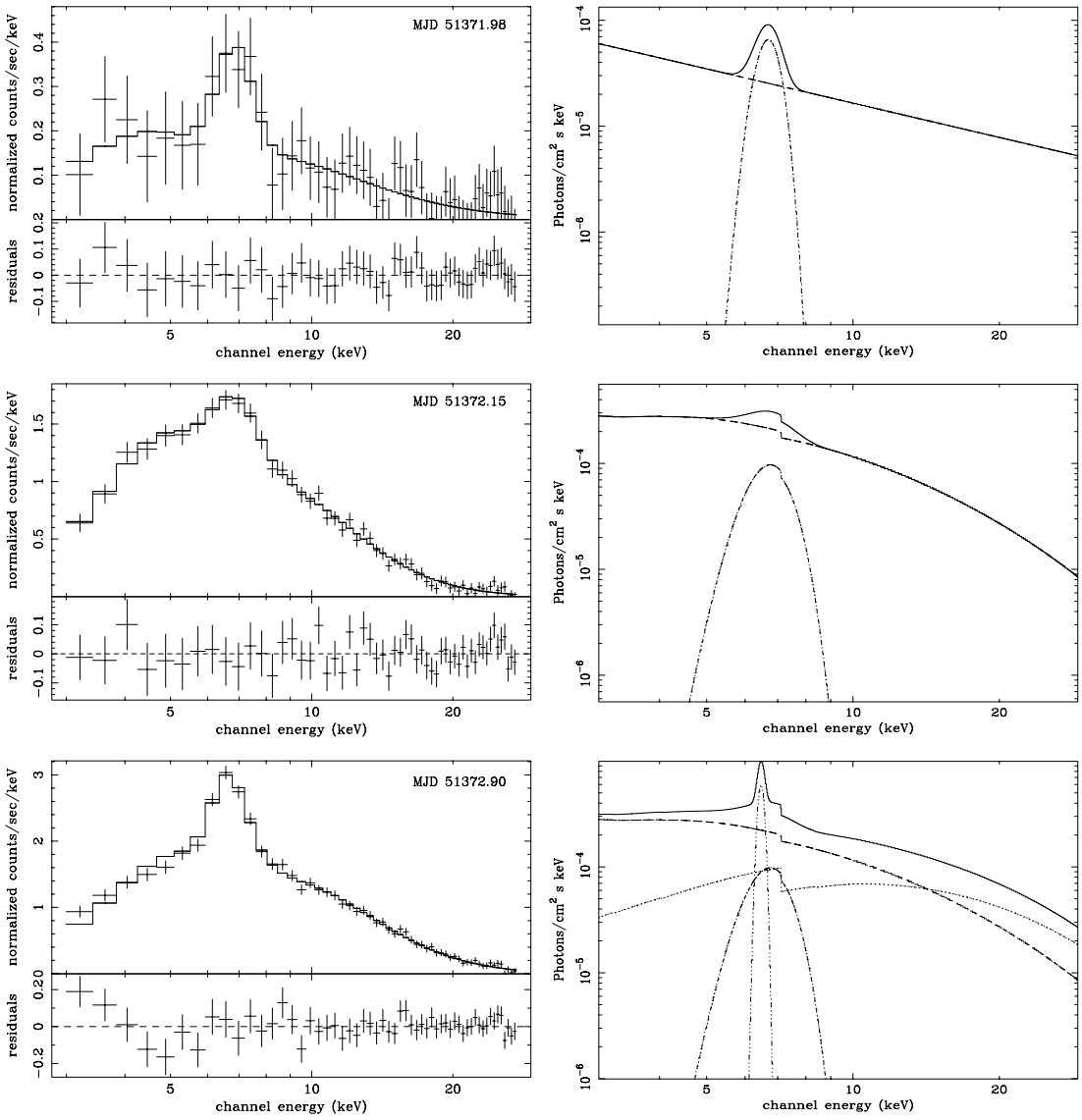

FIG. 4.—Spectral fits from three visits to Her X-1. *Top left panel*: Power law-plus-Gaussian profile fit to mideclipse data (MJD 51,371.98); *top right panel*: best-fit model; *middle panels*: corresponding fit and model of the corona for the posteclipse visit at MJD 51,372.15, consisting of an exponentially cut off power law and line absorbed by a partial cover; *bottom panels*: the visit at maximum flux, MJD 51,372.90, where a reflection component and a second line are added. See § 4 for details of the spectral models.

from § 3. This rather false constraint will allow us to separate approximately the two spectral components and is probably valid across neighboring visits, but not over a number of orbital cycles (Fig. 3).

The visit at MJD 51,372.15 is the most likely to isolate the coronal component. Eclipse egress is approximately complete, and any contribution from the reflection component is assumed negligible. We refrain from using the pre-eclipse visits at MJD 51,373.4 and MJD 51,375.2 in case dipping is occurring. An absorbed power-law model of the form

$$S(E) = \exp\,[-N_{\rm H}\,\sigma(E)]AE^{-\alpha}\,, \qquad (4)$$

where A is the normalization, $\sigma(E)$ the photoelectric cross section (Bałucińska-Church & McCammon 1992), and $N_{\rm H}$ the neutral hydrogen column density, provides an inadequate fit of $\chi^2_{\rm red} = 2.06$ for 54 dof. The addition of a Gaussian model,

$$G(E) = \frac{A_{\rm K}}{(2\pi\sigma_{\rm K}^2)^{1/2}} \exp\left[-\frac{1}{2}\left(\frac{E - E_{\rm K}}{\sigma_{\rm K}}\right)^2\right], \qquad (5)$$

representing an iron emission complex at 6.4–6.7 keV, improves the fit to $\chi^2_{\rm red} = 1.15$ for 51 dof. $A_{\rm K}$ is the line flux, $\sigma_{\rm K}$ the line width, and $E_{\rm K}$ the line center. Compared with previous observations of Her X-1 in anomalous low states (see, e.g., Oosterbroek et al. 2000; Coburn et al. 2000), the power-law component is rather steep, $\alpha = 1.8 \pm 0.1$, and the Fe line is nested at a high-energy level, 6.9 ± 0.2 keV. With further complexity introduced into the model, both the power-law slope and line energy agree with previous results, but the χ^2 statistic cannot discriminate between a number of models. A definitive model is not essential, because these fit parameters will remain fixed in order to extract approximately the reflection spectrum a few visits later. Therefore

TABLE 1

BEST-FIT PARAMETERS FOR THE THREE SPECTRA PRESENTED IN FIG. 4

Parameter	Value
Eclipse parameters:	
α	1.2 ± 0.4
A (photons cm^{-2} s^{-1} keV^{-1})	$(2 \pm 1) \times 10^{-4}$
E_K (keV)	6.7 ± 0.3
σ_K (keV)	0.3 ± 0.2
A_K (photons cm^{-2} s^{-1})	$(6 \pm 3) \times 10^{-5}$
Coronal parameters:	
N_H ($\times 10^{22}$ cm^{-2})	16 ± 12
f	0.7 ± 0.6
α[a]	0.9
E_{cut} (keV)	11 ± 2
A (photons cm^{-2} s^{-1} keV^{-1})	$(3 \pm 1) \times 10^{-3}$
E_K (keV)	6.7 ± 0.2
σ_K (keV)	0.7 ± 0.4
A_K (photons cm^{-2} s^{-1})	$(2 \pm 1) \times 10^{-4}$
Reflection parameters:	
α[a,b]	0.9
E_{cut} (keV)[a,b]	11
A (photons cm^{-2} s^{-1} keV^{-1})[b]	$(9.0 \pm 0.9) \times 10^{-2}$
ω[a]	0.15π
cos θ^a_{obs}	1
cos θ^a_{min}	1
cos θ^a_{max}	0
Fe abundance (solar)[a]	1
f_{esc}[a]	0
E_K (keV)	6.5 ± 0.1
σ_K (keV)	0.1 ± 0.1
A_K (photons cm^{-2} s^{-1})	$(1.5 \pm 0.2) \times 10^{-4}$

NOTES.—All fits are also subject to a fixed interstellar column density of 5.1×10^{19} cm^{-2} (Dal Fiume et al. 1998). The reflection parameters are given for MJD 51,372.90.

[a] Frozen parameter.

[b] Model component is directly invisible to the observer.

we choose a model that is simple but physically realistic and is also compatible with fits made earlier in the anomalous low state by Coburn et al. (2000): in this case a power law with high-energy exponential cutoff, an Fe emission line, and a partial-covering, cold absorber,

$$S(E) = P(E)[A \exp(-E/E_{cut})E^{-\alpha} + G(E)], \quad (6)$$

where

$$P(E) = (1 - f) + f \exp[-N_H \sigma(E)], \quad (7)$$

f is the partial-covering fraction, and E_{cut} the cutoff energy. The excessive number of free parameters means that the column density, covering fraction, and power-law slope are poorly constrained. Because the current anomalous low state is thought to be the result of obscuration, rather than of intrinsic source behavior, we can assume that the coronal photons have undergone elastic scattering and rationalize fixing the power-law slope to its main high-state value, $\alpha = 0.9$ (Dal Fiume et al. 1998). From the visit at MJD 51,372.15, $N_H = (1.6 \pm 0.8) \times 10^{23}$ cm^{-2}, $f = 0.7 \pm 0.1$, $E_{cut} = 11 \pm 2$ keV, $A = (2.6 \pm 0.9) \times 10^{-3}$ photons cm^{-2} s^{-1} keV^{-1} at 1 keV, $E_K = 6.7 \pm 0.1$ keV, and $\sigma_K = 0.7 \pm 0.2$ keV, with a line strength of $(2 \pm 1) \times 10^{-4}$ photons cm^{-2} s^{-1}. $\chi^2_{red} = 0.85$ for 50 dof, and the equivalent width of the Fe complex is 775 eV.

We apply this same model to a visit at $\phi_{orb} = 0.5$ (MJD 51,372.90). Keeping α and E_{cut} fixed at their previous values provides a poor fit, $\chi^2_{red} = 2.74$ for 51 dof. Relaxing both these constraints yields an acceptable fit of $\chi^2_{red} = 0.74$ for 49 dof. However, $N_H = 0$ and α is extremely flat, 0.13 ± 0.12. Consequently, in a time-variable capacity the coronal model alone does not fit the data sensibly. Therefore, a two-source model is more appropriate.

4.2. *Reflection Spectrum*

We would like to test whether reflection provides a good fit to the modulated component. Reflection would be the result of the scattering of hard radiation from the accreting source off the relatively cold atmospheres of the companion star or accretion disk. The spectrum will suffer photoelectric absorption at energies less than 10 keV, will have a strong Fe Kα line, and will be downscattered at energies higher than 50 keV. Thus, the reflection spectrum has a maximum in the *RXTE* PCA band at energies 15–20 keV.

As explained in the previous section, we assume that the coronal model parameters are time-invariant, except for the normalization, which is scaled by the light-curve fit of equation (3). This is in order to reduce the number of free parameters, which is excessive for the quality of spectra from individual visits.

The visit we consider is at $\phi_{orb} \simeq 0.5$ (MJD 51,372.90) and has a number of advantages over other observations. This phase provides the best counting statistics. Furthermore, we expect to be observing $\sim 100\%$ of the irradiated surface at this time, so we can assume that all reflected flux is recorded. Finally, we are reasonably close to the visit in which the coronal spectrum was characterized, and so our assumptions concerning the form and brightness of this component are hopefully valid. We test these assumptions in § 6.

We first attempt adding a few simple models to the coronal component in an attempt to produce a statistically acceptable fit. A second Gaussian component is always required. Adopting $S(E)$ plus power law plus Gaussian provides a $\chi^2_{red} = 1.17$ for 52 dof. The photon index is flat, $\alpha = 0.33 \pm 0.1$, and the fit yields a notable low-energy excess. An $S(E)$ plus blackbody plus Gaussian yields $\chi^2_{red} = 0.72$ for 52 dof. The blackbody temperature is 6.2 ± 0.7 keV, and the 6.4 ± 0.1 keV line has an equivalent width of 3.13 keV. Despite the good fit, it is not obvious what would radiate thermally at this temperature within the framework of the anomalous low-state model (Vrtilek et al. 2001) or produce such a broad line. The low-energy excess remains a feature.

More realistically, we fit $S(E)$ plus Gaussian plus the elastic, cold Compton reflection model HREFL. Although the geometry of this model is more suited to disk reflection than that of a Roche surface, it is the most appropriate model within the XSPEC package and yields an approximate fit. This provides confidence in a more sophisticated approach undertaken in § 6.

The fraction, f_{esc}, of direct X-rays observed is zero, because the point source is obscured by the accretion disk. However, much of the companion-star atmosphere has a largely unobscured view of the X-ray source. The reflection model assumes an isotropically radiating point source of a given energy spectrum and flux that irradiates a structure subtending a solid angle ω on the sky with respect to the point source. By adopting stellar masses of $M_{ns} = 1.4\ M_\odot$ and $M_{com} = 2.2\ M_\odot$ and companion radial velocity of 100

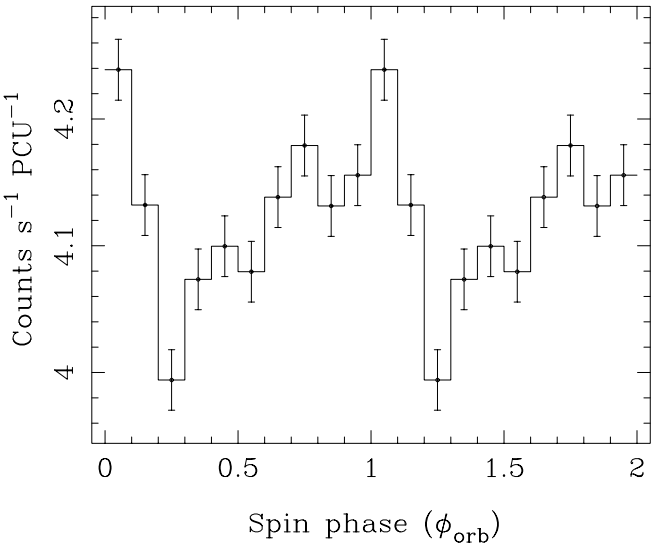

FIG. 5.—Time-averaged spin pulse from Her X-1. The pulse cycle is repeated for clarity.

km s^{-1} (Reynolds et al. 1997), we find $\omega = 0.15\pi$. We approximate a reflecting structure incident to X-rays at all angles between $\theta_{min} = 0°$ and $\theta_{max} = 90°$, weighted equally and inclined on the sky at an angle $\theta_{obs} = 0°$ to the observer at $\phi_{orb} = 0.5$ and orbital inclination $i \simeq 90°$. Solar abundances were adopted. The incident energy spectrum is modeled by the same cutoff power law as before, with $\alpha = 0.9$ and $E_{cut} = 11$ keV.

The photon flux of the irradiating power-law spectrum and Gaussian profile provide just four free parameters, yielding a χ^2_{red} of 0.89 for 53 dof. Fit parameters are listed in Table 1. The fit is extremely good, considering there is only one free parameter available to define the reflection continuum. Encouragingly, photon flux for the unseen power-law source at 1 keV is $(9.0 \pm 0.9) \times 10^{-2}$ photons cm^{-2} s^{-1} keV^{-1}. The flux from a typical high state of Her X-1 is 0.1 photons cm^{-2} s^{-1} keV^{-1} at 1 keV (Dal Fiume et al. 1998). The line is strong, narrow, and nested at low Fe Kα energies, as predicted by reflection models (Basko et al. 1974; Ross & Fabian 1993). This consistency, combined with the period and phasing of the modulated component, points to the companion star providing the reflective surface.

4.3. *Eclipse Spectrum*

The visit during mideclipse (MJD 51,371.98) is fitted well with a single power law, $\chi^2_{red} = 0.93$ for 26 dof over channels 8–35 (3–15 keV). Although the inclusion of an Fe line is not formally required, there is an excess longward of the Fe K edge. Including a Gaussian model suggests a line of equivalent width 2.6 keV, where $\chi^2_{red} = 0.39$ for 23 dof. Here $\alpha = 1.2 \pm 0.3$, $A = (2 \pm 1) \times 10^{-4}$ photons keV^{-1} cm^{-2} s^{-1} at 1 keV, $E_K = 6.7 \pm 0.3$ keV, and $\sigma_K = 0.3 \pm 0.2$ keV, with a line intensity of $(6 \pm 3) \times 10^{-5}$ photons cm^{-2} s^{-1}. Adopting a cutoff power-law model of $\alpha = 0.9$ and $E_{cut} = 11$ keV and fitting just the normalization and line parameters yield consistent Gaussian characteristics within the uncertainties.

5. PULSE TIMING

In this section we report the detection of spin pulses, measure their frequency, and present pulse profiles. Good-Xenon data were extracted over all energy channels and binned to 0.02 s. Times were corrected to the compact sources' local standard of rest using the orbital time delay semiamplitude determined by Deeter et al. (1991), and the spin period of the pulsar was searched for using the Lomb-Scargle algorithm. A period of 1.237746 ± 0.000001 s was found, with a false-alarm probability of 10^{-5}. This is consistent with the measurements of Oosterbroek et al. (2000) and Coburn et al. (2000) during the same anomalous low state, and it signifies that the pulsar has spun down during the low-state episode, as it has in the previous two recorded anomalous low epochs (Vrtilek et al. 1994). Coburn et al. (2000) discuss the implications of these spin-down episodes with regard to the accretion torque in the system. The pulse profile is presented in Figure 5.

It is unlikely that the observed pulses are within reflected light from the companion star. The spin frequency is constant in the rest frame of the compact object, so photons should be scattering off the accretion disk or accretion disk corona. Pulse fractions are of the order a few percent, whereas models of reflected pulses off the companion predict fractions an order of magnitude less (Middleditch & Nelson 1976).

6. MODELING ROCHE LOBE REFLECTION

The reflection models currently available in XSPEC v. 11 are not well suited to our problem. These were developed for accretion-disk reflection problems (see, e.g., Magdziarz & Zdziarski 1995) and limit our results because of incorrect geometry. The available models assume that the reflecting body is a uniform slab, viewed at an inclination angle and illuminated by a point source above the surface of the slab. The size of the slab and the distance from the point source are characterized by a filling factor—the fraction of sky occupied by the slab with respect to the source. The model adopted in § 4.2 takes into account a range of equally weighted irradiance angles to approximate the curved Roche surface of the star, but it is again a simplification of the problem (although a valuable consistency check for more sophisticated models). The simplified model did indicate, however, that the reflected flux was identical (within the 1 σ measurement uncertainty) to that expected from a point source with the distance, energy spectrum, and intensity of Her X-1 at the peak of its high state. We would like to test this more rigorously by defining an accurate reflection surface.

In order to treat the problem more accurately we develop a code which divides the surface of a Roche lobe-filling star into small, discrete elements. Each has an individual inclination angle with respect to the Earth. Each has an individual grazing incidence angle and filling factor with respect to the X-ray source. Our task is to determine these parameters over a grid using Roche geometry and to sum the reflection spectrum over all observer-visible surface elements. This approach both treats the geometry correctly and allows a fit to be made at any orbital phase. Again, we follow the algorithm described in the Appendix.

The model was developed as an external, multiplicative XSPEC package and applied to the spectrum sampled at MJD 51,372.90, where we fitted the composite model of equation (6) by replacing the HREFL component and adopting the fixed coronal and pulsar parameters listed in Table 1. Our reflection parameters are stellar mass ratio $q = M_{com}/M_{ns}$, which defines the shape of the companion

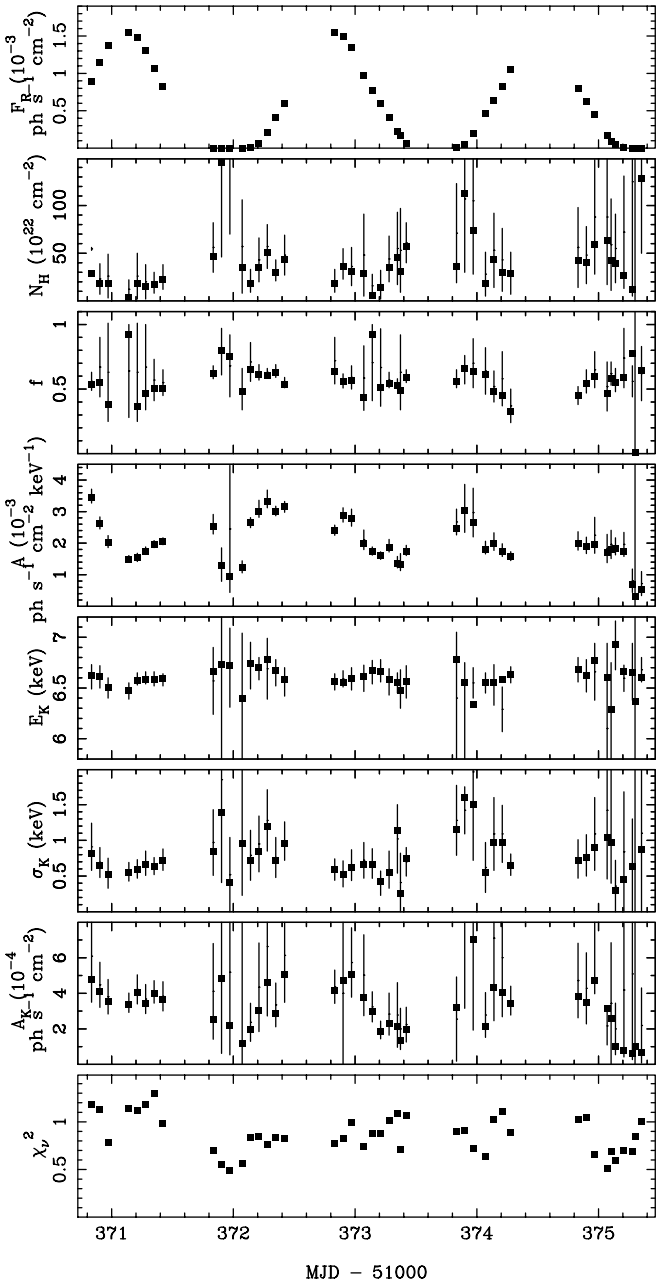

FIG. 6.—The top panel presents the predicted 3–30 keV reflected flux from the companion star as a function of MJD. The remaining panels illustrate the fit parameters of the coronal continuum model and a single Gaussian fitting both coronal and reflected Fe components after the reflection continuum has been subtracted. The bottom panel provides the reduced χ^2-value for each fit.

star and the area of pulsar sky each surface element occupies, the orbital inclination, i, and the orbital phase, $\phi_{\rm orb}$, which together define those elements of the stellar surface visible to Earth. We use the spectroscopic measurements of Reynolds et al. (1997), $q = 1.57$ and $i = 82°$. The orbital ephemeris of equation (1) indicates $\phi_{\rm orb} = 0.55$. In order to calculate the scattering probability the Fe abundance is adopted as solar.

As before, four free parameters remain, yielding a reduced χ^2 of 0.86 for 53 dof, where $A = (9.6 \pm 0.5) \times 10^{-2}$ photons s^{-1} cm^{-2} keV^{-1} at 1 keV, $E_{\rm K} = 6.5 \pm 0.1$ keV, $\sigma_{\rm K} = 0.1 \pm 0.1$ keV, and $A_{\rm K} = (1.4 \pm 0.2) \times 10^{-4}$ photons s^{-1} cm^{-2}. This is consistent with the HREFL model and also confirms that the intrinsic flux from the pulsar is reproduced with reflection off a Roche surface at this orbital phase.

At $\phi_{\rm orb} = 0.5$ the Roche reflection model most resembles the disk reflection models. Ideally, we would like to apply the above test to all orbital phases, but Figure 3 indicates that if stellar reflection drives the orbital light curve, then the coronal spectrum is variable and our model assumptions break down. The alternative approach is to freeze A, calculate the reflection spectrum at each visit, and then fit the coronal model to the residuals.

Because it is not possible to separate the coronal and reflected Fe lines, these are fitted with just a single Gaussian. Neglecting the short-term behavior of the absorbing column and coronal line flux, we expect Gaussian strength, $A_{\rm K}$, and width, $\sigma_{\rm K}$, to vary with the reflection continuum, as a result of the narrow fluorescence line from the companion star varying over the orbital cycle. The 3–30 keV reflection flux (*top panel*) and the best-fit parameters for all visits are presented in Figure 6. Both the coronal α and $E_{\rm cut}$ were frozen during the fits.

Coronal parameters are expected to vary on the 35 day rather than the 1.7 day cycle, and we see no detectable orbital coherency in $N_{\rm H}$, f, or A. The decay of the coronal flux appears related to a long-term increase in $N_{\rm H}$, rather than to a decrease in A, which is consistent with the 35 day disk precession model for Her X-1 (Scott & Leahy 1999). As predicted, $A_{\rm K}$ is modulated on the orbital period, with a maximum at $\phi_{\rm orb} \simeq 0.5$, although similar coherency is not discernible in $\sigma_{\rm K}$.

7. DISCUSSION

Despite the reflection effect in Her X-1 being observed in the EUV band (Leahy & Marshall 1999; Leahy et al. 2000), this is the first convincing detection of the phenomenon at X-ray energies. Basko et al. (1974) demonstrated that X-ray–reflected flux from the companion star in Her X-1 should be at a few percent of the intrinsic radiation. This should generally be washed out by shot noise from the central source during normal high states, but, as in the current observations, it should also be observable during normal low states of the 35 day cycle. Sheffer et al. (1992) claimed a tentative detection of reflection during a normal off state during the *ASTRON* mission, but a systematic search for this effect during normal or anomalous low states has never been undertaken; the HEASARC archive is not rich in data from these epochs, and those that exist coincide with eclipses of the pulsar (see, e.g., Choi et al. 1997). Exceptions are the *EXOSAT* pointings by Parmar et al. (1985), the *BeppoSAX* observations of Oosterbroek et al. (2000), and the *RXTE* visits by Coburn et al. (2000). None of these analyses consider reflection as a possible interpretation of data, but the count rates presented by Parmar et al. (1985) and Oosterbroek et al. (2000) arguably both display 1.7 day modulation. The baseline of the Coburn et al. (2000) visits is 20 ks, covering $\phi_{\rm orb} = 0.64$–0.77. The general trend in count rate over this period is one of decline, as predicted by the reflection model (Fig. 3), although the count rate and decline are a factor of 2 larger than the current data.

Potentially, Her X-1 contains a rich lode of reflection physics. The reflection effect is common to a large number of different X-ray sources, such as AGNs and stellar-mass black holes (Lightman & White 1988; White et al. 1988). But generally there is uncertainty concerning the physical location and size of hard radiation sources in these objects,

and the size and shape of the reflecting atmosphere (which in these cases is presumably an accretion disk). Therefore Her X-1 is an ideal X-ray source for studying the properties of reflection and associated processes (such as winds and coronae), because we have a relatively clear picture of companion-star geometry and its illumination by well-measured hard radiation from a central object.

Despite this there are some limitations. First, it is not clear how, or whether, the X-ray emission from the pulsar is beamed or how column density changes with disk inclination angle. Although the high inclination of the binary means that the observer has a similar line of sight to the source as the equatorial regions of the companion star, surface elements closer to the stellar poles may perceive the central source differently. In this paper we have assumed that the source is an isotropic emitter. Also we assume that the X-ray source is pointlike. This is not true, because we observe scattered light from a disk corona and expect further scattering and reflection from the disk itself; Leahy (1995), using eclipse timings, showed that soft photons come from an extended region. Furthermore, we made no attempt to model the accretion-disk shadow or its eclipse over the equatorial regions of the companion star, because the disk shape is so poorly constrained. The reflection process itself is also treated simply. More sophisticated models (by, e.g., Ross & Fabian 1993 and Nayakshin 2000) consider the physical response of an atmosphere to irradiation and the resultant spectral changes.

There is scope for much more observation. The reflection model can be tested more sensitively with improved models and greater energy resolution using grating spectrometers. These are sensitive to soft energies below 1 keV, which should be populated by resonance absorption edges (Basko et al. 1974), and over the Fe α complex, where they can resolve and separate line components between corona and companion star. In order to constrain the location of reflection, timing experiments with improved sampling over the 35 day cycle would determine whether light-curve modulation is driven on the orbital (1.7 day) or beat (1.6 day) period. Fast timing visits during eclipses of the companion by the accretion disk at $\phi_{\rm orb} = 0.5$ can help constrain the shape of the accretion disk using the eclipse ingress and egress profiles.

8. CONCLUSION

Over 2.7 orbital cycles during the anomalous low state of 1999 the X-ray pulsar Her X-1 displayed an X-ray light curve very similar to optical and UV counterparts, suggesting that the companion star contributes to X-ray emission. A cold Compton reflection spectrum was successfully fitted to the variable component of the energy spectrum. By employing binary geometry and assuming companion-star reflection, the intensity of the hidden pulsar was found to be identical to that of the high state of the source when the pulsar is visible. This result indirectly implies that the anomalous low-state model is correct—intrinsic accretion luminosity remains constant but is occulted along the observer's line of sight by the accretion disk.

This work was funded by NASA grants NRA-99-01-ADP-108, NAG 5-6711, and NAG 5-7333. K. O., K. H., and H. Q. acknowledge support from the Particle Physics and Astronomy Research Council. This research has made use of data obtained from the High Energy Astrophysics Science Archive Research Center (HEASARC), provided by NASA's Goddard Space Flight Center.

APPENDIX A

CLASSICAL COMPTON REFLECTION OFF A ROCHE LOBE-FILLING SURFACE

In order to estimate the stellar reflected flux, one must know the fraction of X-rays intercepted by the atmosphere of the companion and also the reflection properties of that atmosphere. The following calculations construct a stellar surface confined by the Roche equipotential surface of a binary of stellar mass ratio $q = M_{\rm com}/M_{\rm ns}$ (§ A1). They then determine the monochromatic Compton-reflected fraction off discrete surface elements and sum the reflected flux in those elements visible to the observer at binary inclination i and binary phase $\phi_{\rm orb}$ (§ A2).

A1. ROCHE GEOMETRY

The critical Roche potential is defined by

$$\Psi_{\rm cr} = \frac{q}{r_{\rm cr}} + \frac{1}{1 - r_{\rm cr}} + \frac{(1 + q)r_{\rm cr}^2}{2}, \tag{A1}$$

where $r_{\rm cr}$ is normalized to the stellar separation and determined by minimizing $|\epsilon_{\rm cr}/(d\epsilon_{\rm cr}/dr_{\rm cr})|$, where

$$\epsilon_{\rm cr} = (1 + q)r_{\rm cr} - 1 - \frac{q}{r_{\rm cr}^2} + \frac{1}{(1 - r_{\rm cr})^2}. \tag{A2}$$

Using a spherical polar coordinate system (r, θ, ϕ), with an origin at the center of mass of the companion star, the stellar surface is divided over θ and ϕ into segments of equal solid angle (see Fig. 7). For any given θ and ϕ, r is determined by minimizing $|\epsilon/(d\epsilon/dr)|$, where

$$\epsilon = \frac{q}{r} + (1 + r^2 - 2r\cos\theta)^{1/2} + \frac{(1 + q)r^2\cos^2\theta}{2} + \sin^2\theta\cos^2\phi + \frac{1}{2(1 + q)} - r\cos\theta - \Psi_{\rm cr}. \tag{A3}$$

Following the approach previously adopted by Rutten & Dhillon (1994) and Still et al. (1997), each surface segment is divided into two, such that the critical Roche surface is completely tiled by N triangles. This provides a better approximation

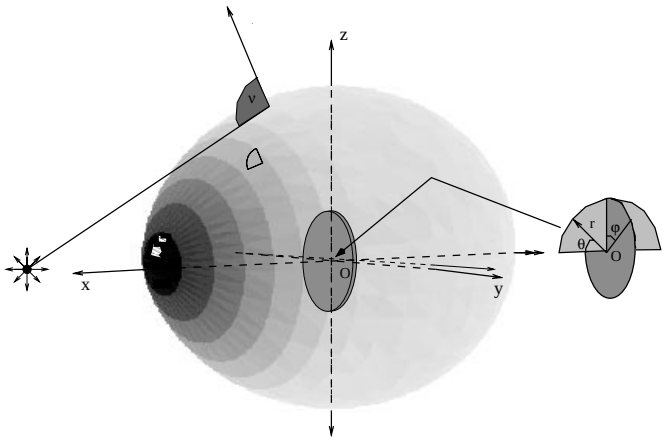

FIG. 7.—Schematic of the geometry used to determine the reflected spectrum. Both Cartesian and polar coordinates are displayed. v is the incidence angle of reflection relative to the neutron star. The incidence angle between surface elements and the observer's line of sight, μ, is the projection angle of each surface element on the page.

to a curved surface than other polygons. The coordinates of each triangle vertex, $V_{jk} = (r_{jk}, \theta_{jk}, \phi_{jk})$, where $j = 1$ to 3 and $k = 1$ to N, are calculated using equations A1–A3 and converted to a Cartesian coordinate system (x_{jk}, y_{jk}, z_{jk}) with an origin at the center of mass, using

$$x_{jk} = r_{jk} \cos \theta_{jk} - \frac{1}{1+q} , \tag{A4}$$

$$y_{jk} = r_{jk} \sin \theta_{jk} \cos \phi_{jk} , \tag{A5}$$

and

$$z_{jk} = r_{jk} \sin \theta_{jk} \sin \phi_{jk} . \tag{A6}$$

The coordinate center of each triangle is $\boldsymbol{T}_k = \sum_{j=1}^{3} (x_{jk}/3, y_{jk}/3, z_{jk}/3)$. The unit vector normal of each triangular surface is

$$\boldsymbol{n}_k = \frac{(\boldsymbol{V}_{2k} - \boldsymbol{V}_{1k})(\boldsymbol{V}_{3k} - \boldsymbol{V}_{1k})}{|(\boldsymbol{V}_{2k} - \boldsymbol{V}_{1k})(\boldsymbol{V}_{3k} - \boldsymbol{V}_{1k})|} , \tag{A7}$$

where the surface area of each element $A_k = |\boldsymbol{n}_k|/2$. The cosine of a surface element's normal vector and the unit direction vector to Earth, $\boldsymbol{e}$, is the incidence angle of reflected photons,

$$\mu_k = \boldsymbol{n}_k \boldsymbol{e} , \tag{A8}$$

where $\boldsymbol{e}$ is defined using the orbital inclination of the binary, i, and the orbital phase, $\phi_{\rm orb}$:

$$\boldsymbol{e}_x = \sin i \cos [\pi(1 - 2\phi_{\rm orb})] , \tag{A9}$$

$$\boldsymbol{e}_y = \sin i \sin [\pi(1 - 2\phi_{\rm orb})] , \tag{A10}$$

and

$$\boldsymbol{e}_z = \cos i . \tag{A11}$$

Similarly, the cosine of each element's normal vector with the unit vector direction to the X-ray source yields the incidence angle of photons arriving at the stellar surface,

$$v_k = \boldsymbol{n}_k \frac{d_k}{|d_k|} , \tag{A12}$$

where

$$d_{x,k} = -T_{x,k} + \frac{q}{1+q} , \tag{A13}$$

$$d_{y,k} = -T_{y,k} , \tag{A14}$$

$$d_{z,k} = -T_{z,k} , \tag{A15}$$

and $|d_k|$ is the distance between the source and each triangle. We assume that the X-ray source is pointlike and is coincident with the center of mass of the pulsar. Finally, the solid angle of sky subtended by each triangle with respect to the X-ray source is

$$\omega_k = v_k \{1 - \cos [\tan^{-1} (\sqrt{A_k/\pi}/|d_k|)]\} . \tag{A16}$$

A2. REFLECTED FLUX

In Chakrabarti & Titarchuk (1995) the reflection problem in a plane geometry was solved exactly using the Fokker-Planck treatment for multiple scattered photons. Photoelectric absorption and downscattering effects were taken into account correctly. They suggest that in the very nonrelativistic energy range, less than 30 keV, the downscattering effects are negligible. Photons scatter off electrons almost coherently, and consequently the results of the classical reflection problem are applicable (Chandrasekhar 1960). If the intrinsic flux spectrum from a point source radiating isotropically from the location of the pulsar is F_E, the reflected flux observed off all surface elements is

$$f_E = \frac{\lambda_E F_E}{2} \sum_{k=1}^{N} \frac{\omega_k \mu_k}{\mu_k + \nu_k} H(\lambda_E, \mu_k) H(\lambda_E, \nu_k) \ (\mu_k > 0, \nu_k > 0) \ . \tag{A17}$$

Unobservable elements with $\mu_k < 0$ and elements not incident to photons from the pulsar, $\nu_k < 0$, should be removed from the sum. λ_E is the photon scattering probability approximated by the piecewise polynomial fit of Morrison & McCammon (1983). $H(\lambda_E, \beta)$ is the classical H function (Chandrasekhar 1960), approximated with an uncertainty of less than 1% using the analytical expression of Basko (1978),

$$H(\lambda_E, \beta) = \frac{1 + \sqrt{3}\beta}{1 + \sqrt{3(1 - \lambda_E)}\beta} \left[1 - \frac{\lambda_E \beta}{4} (1 + \lambda_E^2)(\ln \beta + 1.33 - 1.458\beta^{0.62}) \right] . \tag{A18}$$

REFERENCES

Bałucińska-Church, M., & McCammon, D. 1992, ApJ, 400, 699
Basko, M. M. 1978, ApJ, 223, 268
Basko, M. M., Sunyaev, R. A., & Titarchuk, L. G. 1974, A&A, 31, 249
Boroson, B., Kallman, T., Vrtilek, S. D., Raymond, J., Still, M., Bautista, M., & Quaintrell, H. 2000a, ApJ, 529, 414
Boroson, B., O'Brien, K., Horne, K., Kallman, T., Still, M., Boyd, P. T., Quaintrell, H., & Vrtilek, S. D. 2000b, ApJ, 545, 399
Coburn, W., et al. 2000, ApJ, 543, 351
Chakrabarti, S., & Titarchuk, L. G. 1995, ApJ, 455, 623
Chandrasekhar, S. 1960, Radiative Transfer (New York: Dover)
Choi, C. S., Seon, K. I., Dotani, T., & Nagase, F. 1997, ApJ, 476, L81
Dal Fiume, D., et al. 1998, A&A, 329, L41
Deeter, J. E., Boynton, P. E., Miyamoto, S., Kitamoto, S., Nagase, F., & Kawai, N. 1991, ApJ, 383, 324
Gerend, D., & Boynton, P. E. 1976, ApJ, 209, 562
Giacconi, R., Gursky, H., Kellogg, E., Levinson, R., Schreier, E., & Tananbaum, H. 1973, ApJ, 184, 227
Leahy, D. A. 1995, ApJ, 450, 339
———. 1997, MNRAS, 287, 622
Leahy, D. A., & Marshall, H. 1999, ApJ, 521, 328
Leahy, D. A., Marshall, H., & Scott, D. M. 2000, ApJ, 542, 446
Lightman, A. P., & White, T. R. 1988, ApJ, 335, 57
Magdziarz, P., & Zdziarski, A. A. 1995, MNRAS, 273, 837
Middleditch, J., & Nelson, J. 1976, ApJ, 208, 567
Morrison, R., & McCammon, D. 1983, ApJ, 270, 119
Nayakshin, S. 2000, ApJ, 534, 718
Oosterbroek, T., Parmar, A. N., Dal Fiume, D., Orlandini, M., Santangelo, A., Del Sordo, S., & Segreto, A. 2000, A&A, 353, 575
Papaloizou, J. C. B., & Terquem, C. 1995, MNRAS, 274, 987
Parmar, A. N., Pietsch, W., McKechnie, S., White, N. E., Trümper, J., Voges, W., & Barr, P. 1985, Nature, 313, 119
Press, W. H., Teukolsky, S. A., Vetterling, W. T., & Flannery, B. P. 1992, Numerical Recipes in C (2d ed.; Cambridge: Cambridge Univ. Press)
Pringle, J. E. 1996, MNRAS, 281, 357
Reynolds, A. P., Quaintrell, H., Still, M. D., Roche, P., Chakrabarty, D., & Levine, S. E. 1997, MNRAS, 288, 43
Ross, R. R., & Fabian, A. C. 1993, MNRAS, 261, 74
Rutten, R. G. M., & Dhillon, V. S. 1994, A&A, 288, 773
Scargle, J. D. 1982, ApJ, 263, 835
Schandl, S. 1996, A&A, 307, 95
Scott, D. M., & Leahy, D. A. 1999, ApJ, 510, 974
Sheffer, E. K., et al. 1992, Soviet Astron., 36, 41
Still, M., O'Brien, K., Horne, K., Hudson, D., Boroson, B., Vrtilek, S. D., Quaintrell, H., & Fiedler, H. 2001, ApJ, in press
Still, M. D., Quaintrell, H., Roche, P., & Reynolds, A. P. 1997, MNRAS, 292, 52
Sunyaev, R. A., & Titarchuk, L. G., 1980, A&A, 86, 121
Tananbaum, H., Gursky, H., Kellogg, E. M., Levinson, R., Schreier, E., & Giacconi, R. 1972, ApJ, 174, L143
Vrtilek, S. D., et al. 1994, ApJ, 436, L9
Vrtilek, S. D., Quaintrell, H., Boroson, B., Still, M. D., Fiedler, H., O'Brien, K. & McCray, R. 2001, ApJ, 549, 522
White, T. R., Lightman, A. P., & Zdziarski, A. A. 1988, ApJ, 331, 939
Zhang, W., Giles, A. B., Jahoda, K., Soong, Y., Swank, J. H., & Morgan, E. H. 1993, Proc. SPIE, 2006, 324